Dependence of Scale Factor on Initial Cloud Size for an Atom-Ball Gyroscope

Bruno Pelle[1], Gregory W. Hoth[1], Stefan Riedl[1], Elizabeth A. Donley[1], and John Kitching[1]

[1]Time and Frequency Division, National Institute of Standards and Technology, Boulder, CO, USA

bruno.pelle@nist.gov

Abstract — **We present an atom interferometer based on an expanding cloud of laser-cooled atoms sensitive to 2-axis rotations and 1-axis acceleration in an effective volume of 1 cm³. We observed spatially resolved fringes by imaging the expanding cloud after short free-fall durations. If the atom cloud does not start as a point source, a bias is introduced in the scale factor that differs from the simple point-source limit. We explored the scale factor deviation experimentally with different initial cloud sizes and will present our understanding of this important systematic.**

Index Terms — **Atomic gravimeter, atomic gyroscope, compact inertial sensor, Point Source Interferometry, scale factor bias.**

I. INTRODUCTION

Light-pulse atom interferometers have demonstrated [1] their ability to realize absolute measurements of rotation and acceleration with state-of-the-art accuracy and sensitivity compared to other technologies. So far these results have largely been implemented in laboratory-size experiments, but current efforts are underway to develop more compact instruments for in-field inertial navigation and geodesy. Usually, counter-propagating atomic sources are required to decouple phase shifts induced by rotation and acceleration [2] which leads to a more complex apparatus. To accomplish this decoupling with a single atomic source, we extend the Point Source Interferometry (PSI) technique realized initially in a 10-meter tower [3] to the compact regime.

II. POINT SOURCE INTERFEROMETRY

In our experiment, we use the usual Mach-Zehnder atom interferometer scheme where we first apply a Raman $\pi/2$-pulse to spatially separate the atomic wavepackets thanks to a momentum transfer on one arm of the interferometer. Then a Raman π-pulse is applied, reversing the wavepacket internal and external states. Finally, a last Raman $\pi/2$-pulse allows the wavepacket recombination when their final positions overlap. The laser phase of each pulse is imprinted on the atom phase, leading to a phase difference [1, 2]

$$\Delta\Phi = \Delta\Phi_{\text{acc}} + \Delta\Phi_{\text{rot}} = \vec{k}_{\text{eff}} \cdot \vec{a}T^2 + 2\vec{\Omega} \cdot (\vec{k}_{\text{eff}} \times \vec{v})T^2, \quad (1)$$

which is imprinted on the final atomic level populations. Here $\vec{k}_{\text{eff}}$ is the transferred momentum to the atom, $\vec{v}$ the atomic cloud's center of mass velocity, T the interrogation time between two Raman pulses, and $\vec{a}$ and $\vec{\Omega}$ the apparatus acceleration and rotation. In PSI, we use the point-source approximation to describe the transverse atomic velocity $\vec{v} = \vec{r}/2T$, with $\vec{r}$ the final transverse atom position, and re-write the now spatially-dependent phase as:

$$\Delta\Phi = \vec{k}_{\text{eff}} \cdot \vec{a}T^2 + \vec{\Omega} \cdot (\vec{k}_{\text{eff}} \times \vec{r})T. \quad (2)$$

Since the cloud contains a range of initial velocities, a rotation of the apparatus will induce a phase gradient in the cloud; while an acceleration will change the overall phase. We use this property to allow a spatially resolved measurement of the interferometer phase to determine both rotation and acceleration. The signal appears in the spatial distributions of the final populations of the hyperfine states $|F = 1\rangle$ and $|F = 2\rangle$ due to the correlation introduced between the internal and external states during a stimulated Raman transition [4].

III. EXPERIMENTAL SET-UP

We realize a 3D magneto-optical trap from a ^{87}Rb vapor inside a glass vacuum cell. We obtain 6×10^6 atoms at 5 μK with approximate Gaussian widths of $\sigma_x = 350$ μm and $\sigma_y = 220$ μm. We then release the atoms from the trap and pump all the atoms in the $|m_F = 0\rangle$ state to avoid sensitivity to magnetic fields at first order. During the free fall, we apply the Mach-Zehnder sequence of light pulses. At the same time, we rotate the retro-reflecting mirror of one of the Raman beams to simulate the rotation of the apparatus. We sketch the interferometric sequence in Fig. 1. The gravity $\vec{g}$ is along $\vec{z}$ but for simplicity the cloud's fall is not shown. The thermal expansion of the cloud leads to multiple interferometer trajectories in the planes (x,z) or (y,z), depending on the
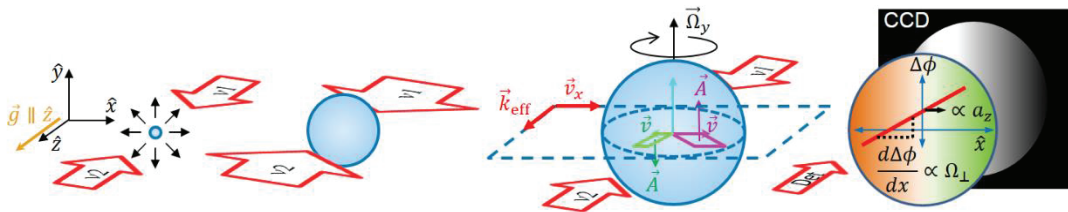

Fig. 1.   Point Source Interferometry scheme in the compact regime.

rotation axis $\vec{\Omega}$. The enclosed area $\vec{A} = \hbar/m \left(\vec{k}_{\text{eff}} \times \vec{v} \right) T^2$, and therefore the rotation phase shift, depends on the atom's initial velocity as shown in panel 3 of Fig. 1. Then the correlation between the atom's initial velocity and final position induces a phase gradient across the atomic cloud. We finally detect the phase gradient by imaging the populations in $|F = 2\rangle$ and in $|F = 1\rangle + |F = 2\rangle$ on a CCD. The CCD is located at the bottom of the glass cell, while the Raman beams are vertically aligned. Thus we measure two rotation axes in the CCD plane (x,y) through the phase gradient and one acceleration axis along the Raman axis ($\vec{z}$) through the phase offset.

IV. SPATIALLY RESOLVED FRINGES

A. Normalized images

We plot in Fig. 2 the ratio image, which corresponds to $R = (N_{F=2} - N_{F=1})/(N_{F=1} + N_{F=2})$ and allows us to suppress the cloud shape, while keeping the fringes visible. The contrast in Fig. 2 is twice the one in transition probability.
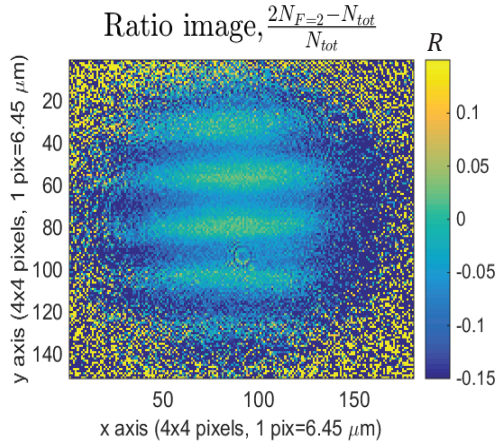

Fig. 2. Spatially resolved interference fringes induced by a rotation $\Omega_x = 136$ mrad/s for a total interrogation time $2T = 16$ ms.
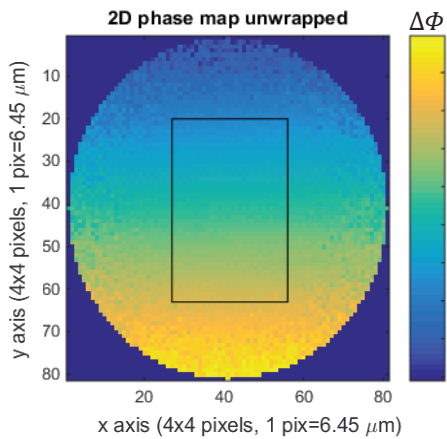

Fig. 3. Extracted phase gradient $k_y = 10.08 \pm 0.1$ rad/mm induced by a rotation of $\Omega_x = 171$ mrad/s for $2T = 16$ ms.

B. Phase gradient extraction

We then reconstruct the phase gradient image in Fig. 3 by scanning the phase offset and fitting a sinusoid for each pixel.

C. Scale factor measurement

In order to determine the scale factor, defined by the slope of k vs Ω, we measure the phase gradients k_x for different rotations. By doing it for two initial cloud sizes, $\sigma_x = 350$ μm and $\sigma_x = 720$ μm, we observe in Fig. 4 an important change in the scale factor corresponding to the impact of the low expansion factor $\sigma_{\text{final}}/\sigma_{\text{initial}} \approx 3$ or 1.5 in a compact regime.
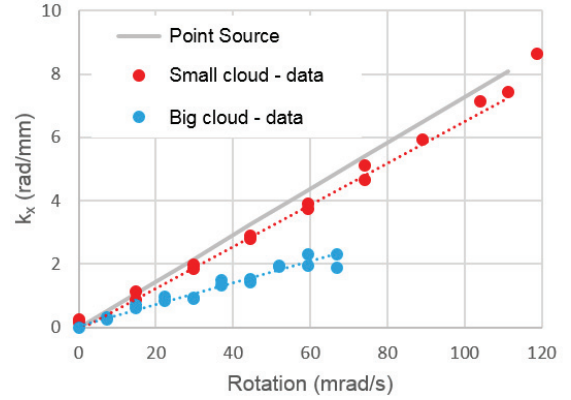

Fig. 4. Scale factor measurement k_x vs Ω_y for two different initial cloud sizes, and the theoretical point-source limit, for $2T = 16$ ms.

V. CONCLUSION

We have seen that spatially resolved fringes can be obtained in a compact regime and that the scale factor is modified by the initial cloud size if the expansion factor is low.

As a mid-term objective, we intend to push toward the interferometer limits. We expect the upper and lower limits of the rotation dynamic range to be set respectively by the atomic cloud's initial size and by atomic shot noise. Then, we will characterize the gyroscope stability with the Earth's rotation.

Ultimately, we hope to develop a compact inertial sensor that would complement other sensing technologies.

REFERENCES

[1] M. A. Kasevich and S. Chu, "Atomic interferometry using stimulated Raman transitions," *Phys. Rev. Lett.,* vol. 67, no. 2, pp. 181 – 184 (1991).
[2] T. L. Gustavson, P. Bouyer, and M. A. Kasevich, "Precision rotation measurements with an atom interferometer gyroscope," *Phys. Rev. Lett.*, vol. 78, no. 11, pp. 2046 – 2049 (1997).
[3] S. M. Dickerson, J. M. Hogan, A. Sugarbaker, D. M. S. Johnson, and M. A. Kasevich, "Multiaxis Inertial Sensing with Long-Time Point Source Atom Interferometry," *Phys. Rev. Lett.,* vol. 111, no. 8, pp. 083001 (2013).
[4] C. J. Bordé, "Atomic interferometry with internal state labelling," *Physics Letters A,* vol. 140, no. 1, pp. 10 – 12 (1989).